



Aalborg Universitet

AALBORG UNIVERSITY
DENMARK

Robust simultaneous myoelectric control of multiple degrees of freedom in wrist-hand prostheses by real-time neuromusculoskeletal modeling

Sartori, Massimo; Durandau, Guillaume; Došen, Strahinja; Farina, Dario

Published in:
Journal of Neural Engineering

DOI (link to publication from Publisher):
[10.1088/1741-2552/aae26b](https://doi.org/10.1088/1741-2552/aae26b)

Publication date:
2018

Document Version
Accepted author manuscript, peer reviewed version

[Link to publication from Aalborg University](#)

Citation for published version (APA):

Sartori, M., Durandau, G., Došen, S., & Farina, D. (2018). Robust simultaneous myoelectric control of multiple degrees of freedom in wrist-hand prostheses by real-time neuromusculoskeletal modeling. *Journal of Neural Engineering*, 15(6), 066026. <https://doi.org/10.1088/1741-2552/aae26b>

General rights

Copyright and moral rights for the publications made accessible in the public portal are retained by the authors and/or other copyright owners and it is a condition of accessing publications that users recognise and abide by the legal requirements associated with these rights.

- Users may download and print one copy of any publication from the public portal for the purpose of private study or research.
- You may not further distribute the material or use it for any profit-making activity or commercial gain
- You may freely distribute the URL identifying the publication in the public portal -

Take down policy

If you believe that this document breaches copyright please contact us at vbn@aub.aau.dk providing details, and we will remove access to the work immediately and investigate your claim.

ACCEPTED MANUSCRIPT

Robust Simultaneous Myoelectric Control of Multiple Degrees of Freedom in Wrist-Hand Prostheses by Real-Time Neuromusculoskeletal Modeling

To cite this article before publication: Massimo Sartori *et al* 2018 *J. Neural Eng.* in press <https://doi.org/10.1088/1741-2552/aae26b>

Manuscript version: Accepted Manuscript

Accepted Manuscript is “the version of the article accepted for publication including all changes made as a result of the peer review process, and which may also include the addition to the article by IOP Publishing of a header, an article ID, a cover sheet and/or an ‘Accepted Manuscript’ watermark, but excluding any other editing, typesetting or other changes made by IOP Publishing and/or its licensors”

This Accepted Manuscript is © 2018 IOP Publishing Ltd.

During the embargo period (the 12 month period from the publication of the Version of Record of this article), the Accepted Manuscript is fully protected by copyright and cannot be reused or reposted elsewhere.

As the Version of Record of this article is going to be / has been published on a subscription basis, this Accepted Manuscript is available for reuse under a CC BY-NC-ND 3.0 licence after the 12 month embargo period.

After the embargo period, everyone is permitted to use copy and redistribute this article for non-commercial purposes only, provided that they adhere to all the terms of the licence <https://creativecommons.org/licenses/by-nc-nd/3.0>

Although reasonable endeavours have been taken to obtain all necessary permissions from third parties to include their copyrighted content within this article, their full citation and copyright line may not be present in this Accepted Manuscript version. Before using any content from this article, please refer to the Version of Record on IOPscience once published for full citation and copyright details, as permissions will likely be required. All third party content is fully copyright protected, unless specifically stated otherwise in the figure caption in the Version of Record.

View the [article online](#) for updates and enhancements.

Robust Simultaneous Myoelectric Control of Multiple Degrees of Freedom in Wrist-Hand Prostheses by Real-Time Neuromusculoskeletal Modeling

Massimo Sartori^{1,*}, Guillaume Durandau¹, Strahinja Došen², and Dario Farina³

¹Department of Biomechanical Engineering, University of Twente, NETHERLANDS
² Department of Health Science and Technology, Faculty of Medicine, Aalborg University, DENMARK
³Department of Bioengineering, Imperial College London, UNITED KINGDOM

*Address of correspondence
Massimo Sartori, Ph.D.
Assistant Professor
University of Twente
TechMed Centre
Faculty of Engineering Technology
Department of Biomechanical Engineering
Building Horsting - Room W106 - P.O. Box 217
7500 AE Enschede, The Netherlands
Email: m.sartori@utwente.nl

Keywords: electromyography; EMG-driven modeling; muscle force; musculoskeletal modeling; myoelectric prosthesis; joint moment; real-time; transradial amputee.

ABSTRACT

Objectives: Robotic prosthetic limbs promise to replace mechanical function of lost biological extremities and restore amputees’ capacity of moving and interacting with the environment. Despite recent advances in biocompatible electrodes, surgical procedures, and mechatronics, the impact of current solutions is hampered by the lack of intuitive and robust man-machine interfaces. **Approach:** Based on authors’ developments, this work presents a biomimetic interface that synthesizes the musculoskeletal function of an individual’s phantom limb as controlled by neural surrogates, i.e. electromyography-derived neural activations. With respect to current approaches based on machine learning, our method employs explicit representations of the musculoskeletal system to reduce the space of feasible solutions in the translation of electromyograms into prosthesis control commands. Electromyograms are mapped onto mechanical forces that belong to a subspace contained within the broader operational space of an individual’s musculoskeletal system. **Results:** Our results show that this constraint makes the approach applicable to real-world scenarios and robust to movement artefacts. This stems from the fact that any control command must always exist within the musculoskeletal model operational space and be therefore physiologically plausible. The approach was effective both on intact-limbed individuals and a transradial amputee displaying robust online control of multi-functional prostheses across a large repertoire of challenging tasks. **Significance:** The development and translation of man-machine interfaces that account for an individual’s neuromusculoskeletal system creates unprecedented opportunities to understand how disrupted neuro-mechanical processes can be restored or replaced via biomimetic wearable assistive technologies.

53 INTRODUCTION

54 The accurate and robust decoding of human limb motor function from recordings of the underlying
 55 neuromuscular activity (i.e. brain, nerve or muscle electrophysiological signals) is a complex, long-standing
 56 problem [1–3]. This challenge is central for the development of control paradigms to restore lost motor
 57 function in impaired individuals. Despite the advances in electromyography (EMG) and in surgical
 58 procedures such as targeted muscle reinnervation [4], myoelectric prostheses still have limited clinical and
 59 commercial impact [5], i.e. upper limb prostheses have peak abandonment rates between 40%-50% and
 60 average rates around 25% among users [2].

61 Current myoelectric prosthesis control methods rely on machine learning where pattern recognition and
 62 linear/non-linear regressions map EMGs into limb kinematics [6,7]. However, the human neuro-musculo-
 63 skeletal system is characterized by multiple muscles spanning a single joint. Therefore, the same joint
 64 rotation can be generated by different EMG patterns that can further vary across individuals, training
 65 conditions, arm postures, or tasks [8]. The mapping functions learned in a specific condition (i.e. low force
 66 tasks, or specific arm posture) do not necessarily generalize to novel conditions (i.e. high force tasks, or
 67 different arm posture). Furthermore, the mapping from EMG to kinematics is not direct, as assumed in
 68 machine learning schemes, i.e. limb kinematics is the musculoskeletal system final output generated by
 69 series of dynamic transformations (transfer functions) in response to control commands (EMG). For this
 70 reason, a single mapping function between EMGs and joint angular position (current state of the art
 71 approaches) may not always capture the complexity of all intermediate nonlinear transformations [2,9].

72 A major barrier to natural artificial limb myoelectric control is the limited understanding of the
 73 biomechanical and neuromuscular mechanisms governing biological joints. Here we propose an interface
 74 that exploits an individual's broader neuro-mechanical information for device control rather than only the
 75 underlying electrophysiological signals [1,10]. We record residual forearm EMGs from a transradial amputee
 76 and intact-limbed individuals, extract EMG-based features of neural activation and concurrently drive
 77 forward a subject-specific musculoskeletal model of the forearm [11–14]. This enables predicting the
 78 resulting mechanical moments actuating wrist-hand joints and prescribing them in real-time to a robotic
 79 multi-functional prosthesis low-level controller.

80 Although recent research demonstrated the possibility of operating EMG-driven musculoskeletal models
 81 in real-time during dynamic movements [15–17], online EMG-driven modelling has never been developed

and applied for the control of multiple degrees of freedom (DOF) robotic limbs. To the best of our knowledge the work presented in this manuscript is the first demonstration of real-time model-based myoelectric prosthesis control on amputee individuals.

Current state of the art work proposed and tested modeling formulations in intact-limbed individuals in isometric conditions and about a single joint DOF, i.e. elbow flexion-extension [18]. Although a real-time two-DOF upper limb model was recently proposed [19], this was not driven by EMGs but operated via simulated signals. A simplified lumped-parameter model of the hand [20,21] was recently used to compute wrist and metacarpophalangeal joint flexion/extension angles in a transradial amputee. However, this did not show the ability of controlling a physical prosthesis in real-time. That is, tests involved non-functional static poses where the amputee controls a virtual cursor to reach given targets [20–22]. This is a major limitation. Without direct proof of physical prosthesis control it is not possible to assess whether a myocontrol method can be realistically employed by the user. Tests based on virtual cursor control would not account for prosthesis weight, socket pressure, and prosthesis interaction with real objects, which would affect EMG quality, stability, and pose a challenge for control. Tests only involving static poses would not account for EMG non-stationarities (due to muscle fiber movement relative to electrode pick up areas), which may further affect control performance. Moreover, these tests would not enable understanding whether reported target reaching times enable prompt control of a physical prosthesis during functional tasks.

Importantly, current model-based methods integrate the dynamic equations of motions in order to predict joint angles from EMGs [19,20,23]. As previously demonstrated [23], the numerical integration problem can become stiff, thus displaying numerical instability in the forward dynamic simulation. As a result, due to numerical integration computational load, state of the art formulations underlie simplified lumped musculoskeletal models with reduced sets of DOFs, limiting translation to more proximal amputations, i.e. transhumeral. These are major elements hampering robustness in the EMG-driven models currently existing, which may underpin the current inability of employing EMG-driven musculoskeletal modeling for the real-time control of robotic limbs.

The authors recently demonstrated the ability to establish real-time EMG-driven musculoskeletal models for the online estimation of joint moments about three DOFs simultaneously in the human lower limb [24]. Based on this work, we here translate and embed a large-scale and physiologically-accurate EMG-driven musculoskeletal model [25] into a new myoelectric control paradigm for a multifunctional robotic wrist-hand

prosthesis. Unlike state-of-the-art approaches, our method does not integrate the equations of motion (Fig. 1A). We propose a new paradigm where the physical prosthesis is used, instead of a numerical integrator [20], to convert EMG-decoded joint moments into joint angles (Fig. 1B-C). Whether or not it is possible to decode phantom limb joint moments, instead of joint angles, from residual muscle EMGs and concurrently control a physical prosthesis represents an unanswered question. If possible, this would enable fast simulation of large-scale musculoskeletal models and open up to applications requiring the control of many DOFs, especially important for individuals who underwent targeted muscle reinnervation procedures.

We here show that our proposed paradigm is robust to arm postures while enabling seamless wrist-hand prosthesis control across a large repertoire of functionally relevant motor tasks in an individual with transradial amputation. We provide tangible results showing the successful use of a new model-based paradigm in real myoelectric prosthesis control scenarios and real-world situations involving patients. The novel method we propose consistently outperformed the classic two-channel control (representing the commercial benchmark) in all the tests including multiple-DOF tasks as well as single-DOF tasks where the commercial benchmark is expected to be best performing. To the best of our knowledge these results have never been achieved by any study so far.

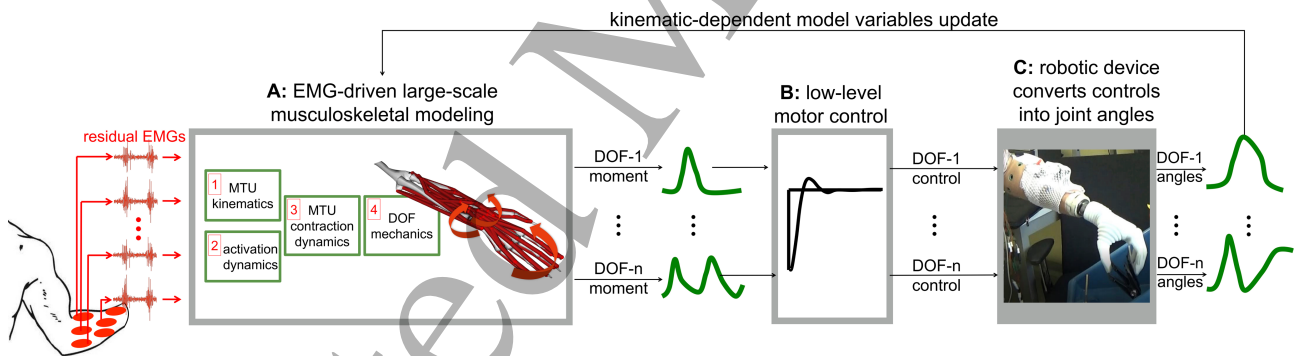


Figure 1. Model-based control schematics for upper limb myoelectric robotic limbs. (A) A large-scale, physiologically correct musculoskeletal model predicts muscle forces of residual forearm muscles as well the resulting joint moments acting on the amputee's phantom limb. (B) Joint moment estimates are converted into prosthesis low-level motor commands. (C) The prosthesis is the physical device that converts EMG-predicted joint forces into joint kinematics, rather than using numerical integration as previously proposed. This enables real-time simultaneous and proportional control multi of multiple degrees of freedom (DOFs) in myoelectric robotic limbs.

1
2 135 **METHODS**

3
4 136 We developed a subject-specific modeling formulation (Figs 1-2) that enabled estimation of wrist-hand
5
6 137 musculoskeletal function in both intact-limbed individuals and transradial amputees as controlled by EMG-
7
8 138 derived neural activations. We demonstrated the ability of using resulting model-based joint moment
9
10 139 estimates for the concurrent, real-time control of a myoelectric prosthesis throughout a large repertoire of
11
12 140 wrist-hand tasks. Our proposed framework schematic is depicted in Figs 1-2 and comprises three major
13
14 141 components including: EMG-driven musculoskeletal model (Fig. 1A), prosthesis low-level controller (Fig.
15
16 142 1B-C), and model calibration (Fig. 2). The EMG-driven musculoskeletal model component is developed
17
18 143 based on previous work from the authors [13–15,26–30] as well as from other groups [31–37].
19
20

21 144 Experimental procedures were performed for each individual subject on two consecutive days. During
22
23 145 the first day, a musculoskeletal model was scaled and calibrated to match each individual’s anthropometry
24
25 146 and force-generating capacity. During the second day, the subject-specific model was employed for the
26
27 147 online prosthesis control tests across arm configurations. Online control tests were performed with no model
28
29 148 re-calibration and involved direct comparison with the classic two-channel control benchmark. The
30
31 149 commercial benchmark was chosen because it provides highest robustness in the control of single-DOFs
32
33 150 across arm configurations and therefore represents the best means for comparison with respect to our
34
35 151 proposed method.
36

37
38 152 First, we describe how motion data were collected and processed for establishing subject-specific
39
40 153 musculoskeletal models, i.e. see Data Recording and Processing Section. Second, we describe our proposed
41
42 154 model-based framework components (see EMG-driven Musculoskeletal Model, Prosthesis Low-Level
43
44 155 Controller and Model Calibration Sections) along with the communication framework that enabled data flow
45
46 156 between EMG amplifier, prosthetic limb and model-based framework (see System Communication
47
48 157 Framework Section). Third we describe the online prosthesis control testing procedures (see Experimental
49
50 158 Tests Section).
51

52
53 159
54
55 160 **Data Recording and Processing**

56
57 161 Motion capture data were recorded (256Hz) using a seven-camera system (Qualisys, Göteborg, Sweden,
58
59 162 256Hz) and a set of 18 retro-reflective markers placed on the individual’s intact left upper extremity, residual
60
163 right upper extremity, trunk, and pelvis. Data were recorded during one static anatomical pose and used in

conjunction with the open-source software OpenSim [38] to scale a generic upper extremity model of the musculoskeletal geometry [25,39] to match the subject's anthropometry. The musculoskeletal geometry model had six upper extremity DOFs including: shoulder elevation, shoulder adduction-abduction, elbow flexion-extension, forearm pronation-supination, wrist flexion-extension, and first-to-fourth proximal metacarpophalangeal joint flexion-extension. Although the model encompasses all DOFs and muscle-tendon units (MTUs) in the human hand [25], only a subset of these were employed. Specifically, this incorporated a total of 12 MTUs spanning the elbow, wrist and hand joints (Table I). During the scaling process, virtual markers were placed on the generic musculoskeletal geometry model based on the position of the experimental markers from the static pose. The model anthropomorphic properties as well as MTU insertion, origin and MTU-to-bone wrapping points were linearly scaled on the basis of the relative distances between experimental and corresponding virtual markers[38].

EMGs were measured (10KHz) and A/D converted with 12-bit precision using a 256-channel EMG amplifier (OTBioelettronica, Torino, IT). Only eight channels were used for the experiment, i.e. via eight pairs of disposable bipolar electrodes (Ambu, Neuroline 720, DK). Electrodes were placed in the correspondence of eight upper limb muscle groups including: biceps brachii, pronator teres, extensor carpi radialis, extensor carpi ulnaris, extensor digitorum, flexor carpi radialis, flexor carpi ulnaris, flexor digitorum. Placement was performed following SENIAM recommendations with a 10mm inter-electrode distance (measured from each electrode center) [40]. Each individual was initially asked to perform maximal voluntary contractions articulating wrist flexion-extension, forearm pronation-supination, and hand opening-closing. EMGs were high-pass filtered (30Hz), full-wave rectified, and low-pass filtered (6 Hz) using a second-order Butterworth filter. Resulting peak-processed values were used for the subsequent EMG normalization during the real-time myocontrol experimental tests. All tests were performed using a powered multi-functional wrist hand prosthesis (Michelangelo Hand, Ottobock HealthCare GmbH, Duderstadt, DE) equipped with wrist pronation-supination (WPS), flexion-extension (WFE) and hand opening-closing (HOC) motors. The prosthesis can produce two grasp types; the palmar grasp was used (HOC) in the present study. The hand is sensorized with embedded position and force sensors, measuring aperture size, wrist rotation angle and grasping force. The commands to the hand and sensor data from the hand were transmitted through a Bluetooth or TCP/IP connection (100 Hz).

Table I. EMG to MTU mapping. Mapping between experimental electromyograms (EMGs) and

simulated musculotendon units (MTUs)*.

EMGs	Biceps Brachii	Pronator Teres	Extensor Carpi Radialis	Extensor Carpi Ulnaris	Extensor Digitorum	Flexor Carpi Radialis	Flexor Carpi Ulnaris	Flexor Digitorum
MTUs	BIClong, BICshort	PT, PQ	ECRL, ECRB	ECU	EDC	FCR	FCU	FDS, FDPM

* Musculotendon unit names: biceps brachii long head (BIClong) and short head (BICshort), extensor carpi radialis longus (ECRL), extensor carpi radialis brevis (ECRB), extensor carpi ulnaris (ECU), extensor digitorum communis (EDC), flexor carpi radialis (FCR), flexor carpi ulnaris (FCU), flexor digitorum superficialis (FDS), flexor digitorum profundus (FDPM), pronator quadratus (PQ), and pronator teres (PT).

EMG-driven Musculoskeletal Model

Our proposed EMG-driven modeling framework (Fig. 1) receives as an input: (1) EMGs from the amputee’s residual limb and (2) prosthesis joint angles. This information is used to compute the mechanical moments produced to actuate the amputee’s phantom limb and the intact-limbed individuals’ wrist-hand. The EMG-driven musculoskeletal modeling formulation comprises four main components [13,26,27,41]. The **neural activation component** (Fig. 1A.1) converts EMGs into MTU-specific activation using a second order muscle twitch model and a non-linear transfer function [13,30,41]. Eight EMG channels were mapped into 12 MTUs as detailed in Table I. The **MTU kinematics component** (Fig. 2A.2) synthesizes the MTU paths defined in the subject-specific geometry model into a set of MTU-specific multidimensional cubic B-splines. Each B-spline computes MTU kinematics (i.e. MTU length and moment arms) as a function of input prosthesis joint angles [27]. The **MTU dynamics component** (Fig. 2A.3) solves for the dynamic equilibrium between muscle fibers and series tendons in the production of MTU force. It employs a Hill-type muscle model with activation-force-length-velocity relationships informed by MTU length and neural activations from the previous two components [13,42]. The **joint mechanics component** (Fig. 1A.4) transfers MTU forces to the skeletal joint level using MTU moment arms. This enables computing joint moments [13]. Unlike state of the art methods, this procedure does not require forward integration of the equations of motion and is done in real-time using a physiologically correct large-scale musculoskeletal model, i.e. no need for simplification in the underlying musculoskeletal structure being modeled [11].

Prosthesis Low-Level Controller

The joint moments predicted by the EMG-driven model are subsequently converted into prosthesis low-level control commands (Fig. 1B). These are first amplitude-normalized, threshold-processed, and prescribed to

the prosthesis DOFs individually (Fig. 1C). The prosthesis embedded low-level controller receives input commands and rotates the prosthesis joints with a velocity profile that is proportional to the decoded joint moment. The prosthesis DOF angular kinematics is directly modulated as a function of the input command amplitude. The prosthesis movement emerging from these commands is fed into the EMG-driven model MTU kinematic component (Fig. 1A.2) and used to update the kinematic-dependent state in the musculoskeletal model. This includes skeletal DOF angular position as well as DOF-angle-dependent MTU length, MTU-to-bone wrapping points, and MTU moment arms.

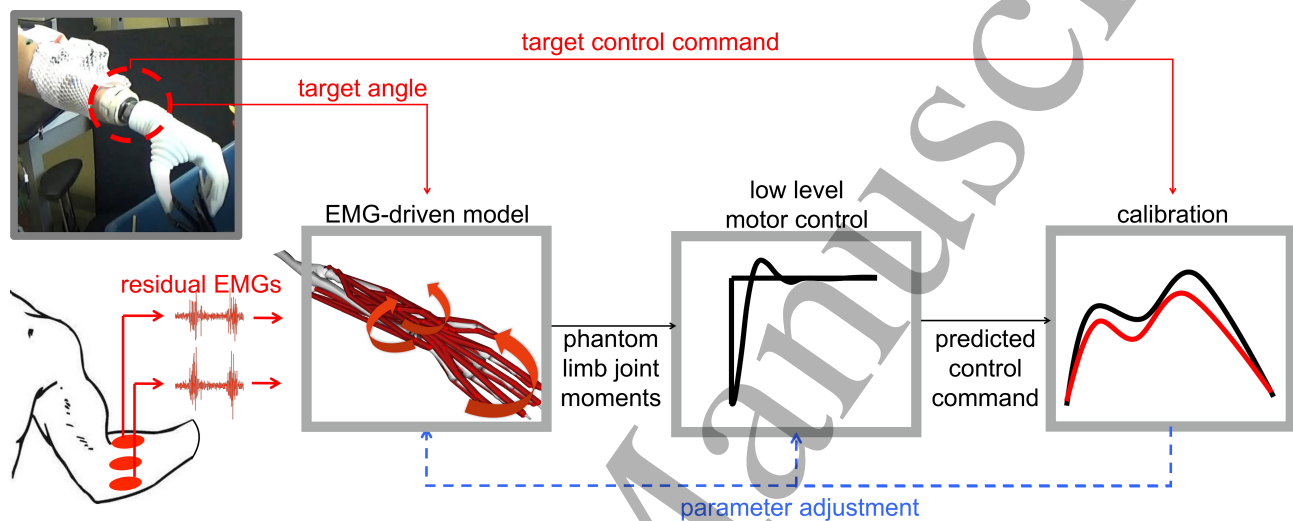


Figure 2. Model calibration procedure. The real-time EMG-driven model-based controller is calibrated using prosthesis joint motor control commands. During calibration the amputee is instructed to mimic pre-defined motions executed by the prostheses using their own phantom limb. EMG-driven model internal parameters are repeatedly refined, as part of a least-squares optimization procedure, so that the mismatch between EMG-driven model's predicted prosthesis DOF commands and those produced by the prosthesis pre-defined command inputs is minimized.

Model Calibration

During calibration, the amputee is instructed to activate the muscles in the residual limb mimicking pre-defined motions executed by the prostheses using their own phantom limb (Fig. 2). Pre-defined prostheses motions to mimic involve moving through the full range of motion about each selected DOF at a constant speed. Pre-defined motions included: wrist flexion-extension, forearm pronation-supination, and hand opening-closing. During this, the calibration algorithm receives three input signals: EMGs from the amputee's residual limb, prosthesis DOF angles, as well as the prosthesis DOF control commands

(normalized velocities) producing the target DOF angles. The **calibration component** (Fig. 2) identifies a number of amputee-specific musculoskeletal parameters that vary non-linearly across individuals because of anatomical and physiological differences. These include: muscle twitch activation/deactivation time constants, EMG-to-activation non-linearity factor, muscle optimal fiber length, tendon slack length, and muscle maximal isometric force. The initial nominal parameters are repeatedly refined, as part of a least-squares optimization procedure, so that the mismatch between EMG-driven model’s predicted prosthesis DOF commands and those applied to the prosthesis (predefined normalized velocities) is minimized. Calibration operates offline using prerecorded data. This enables calibration of both uni-lateral and bi-lateral amputees, since the subject mirrors the movement of the prosthesis with the phantom limb (instead of mirroring the contralateral healthy limb as in [20]).

System Communication Framework

The whole real-time modeling framework (i.e. EMG-driven Model and Calibration, Figs 1-2) operated on a laptop with dual-core processing unit (2.60GHz) and 16GB of RAM memory. Based on our recent work [24] we developed two software plug-in modules that enabled direct TCP/IP connection between the real-time modeling framework and external devices. The first plug-in module provided a direct TCP/IP connection to the external EMG amplifier. It recorded the raw EMGs and processed them as described in the Data Recording and Processing Section. The second plug-in module enabled a direct TCP/IP connection to the prosthetic limb. It processed the EMG-driven model-based estimates of wrist-hand moments to produce prosthesis low-level control commands, i.e. see Prosthesis Low-Level Controller Section.

Table II. Description of subjects investigated. Intact-limbed subjects are labeled as IL1-3. The transradial amputee individual is labeled as TR1.

	Age (Years)	Weight (Kg)	Height (cm)	Sex	Number of electrodes used	Amputation Level	Years since amputation	Prosthesis use
IL1	34	68	183	Male	8	-	-	-
IL2	26	73	177	Male	8	-	-	-
IL3	40	73	176	Male	8	-	-	-
TR1	50	75	168	Male	8	Transradial	30	Daily

Experimental Tests

Experiments were conducted in accordance with the declaration of Helsinki. The University Medical Center Göttingen Ethical Committee approved all experimental procedures (Ethikkommission der

Universitätsmedizin Göttingen, approval number 22/4/16). Three intact-limbed individuals (IL1-3) and one transradial amputee (TR1, Table II) volunteered for this investigation after providing signed informed consent form. Amputation in the TR1 individual was a result of a traumatic injury at year 20th (Table II). Residual stump was estimated to be of 15 cm as measured from the stump most distal point to elbow lateral epicondyle. The TR1 individual is a regular prosthetic user currently fitted with a myocontrolled prosthesis (Michelangelo Hand, OttoBock HealthCare, GmbH) and the two-EMG-channel direct control scheme also used in our tests. None of the subjects had any neuromuscular disorder or abnormality than listed. Subjects performed three series of tasks including: virtual target reaching, clothespin, and functional tests. All tests were performed with no force feedback provided to the amputee.

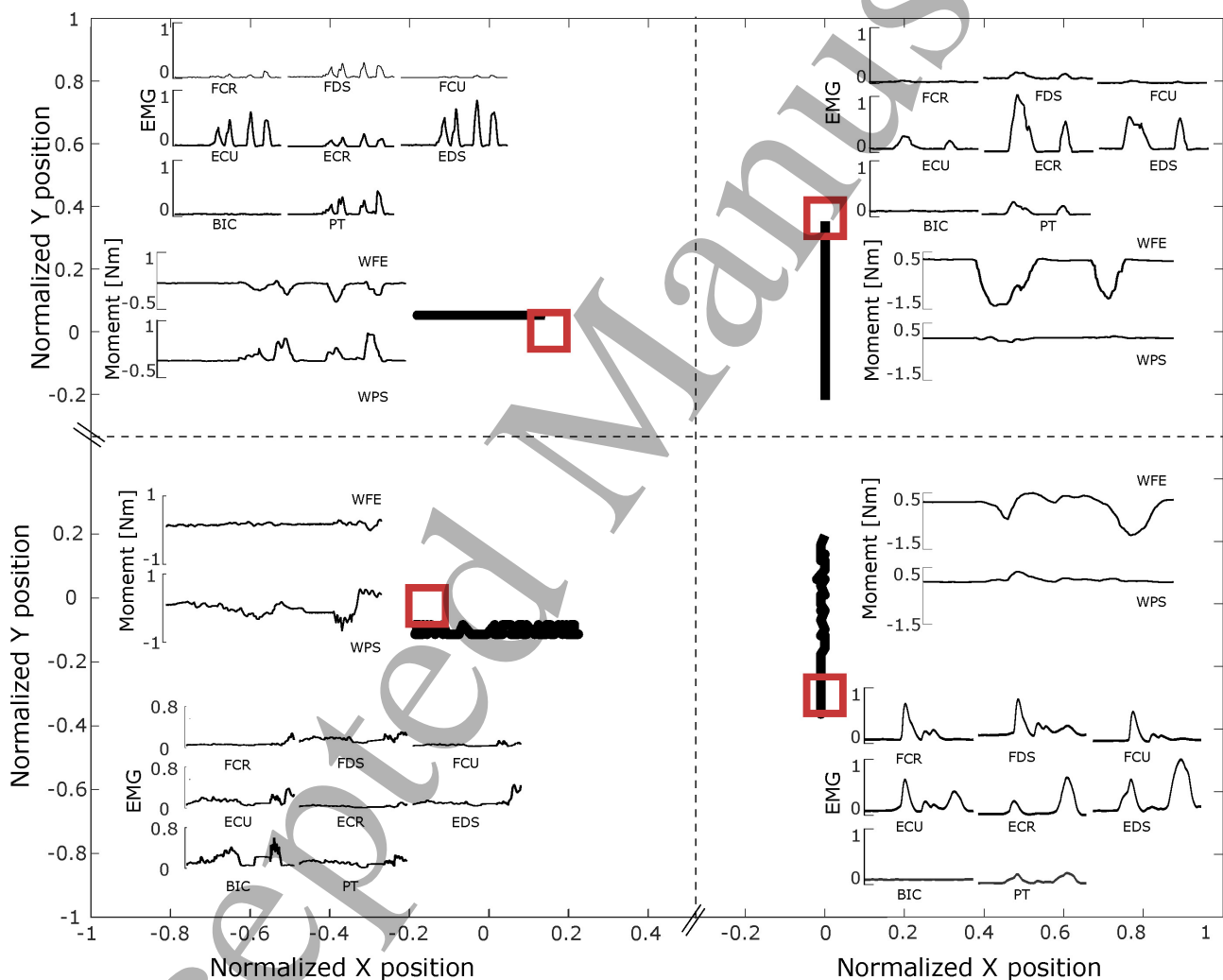


Figure 3. Vertical and horizontal target reaching tests reported for the transradial amputee (TR1).

Four representative target positions to reach are depicted as red square-shaped cursors. The target workspace spanned the interval $[-1, 1]$ in normalized units in both vertical and horizontal directions, where -1 and 1 corresponded to full pronation/flexion and supination/extension of the prosthesis. Vertical targets are

accomplished by operating the prosthesis wrist flexion-extension (WFE) degree of freedom (DOF). Horizontal targets are accomplished by operating prosthesis forearm pronation-supination (WPS) DOF. Each target is represented along with the underlying electromyograms (EMGs) recorded from the residual forearm muscles including: flexor/extensor carpi radialis (FCR/ECR), flexor/extensor carpi ulnaris (FCU/ECU), flexor/extensor digitorum superficialis (FDS/EDS), pronator teres (PT), and biceps brachii (BIC). Furthermore, the resulting DOF moments predicted at the phantom limb WFE and WPS DOFs are depicted, i.e. see black curves in each quadrant. EMGs are depicted as dimensionless curves whereas moments are represented in Nm.

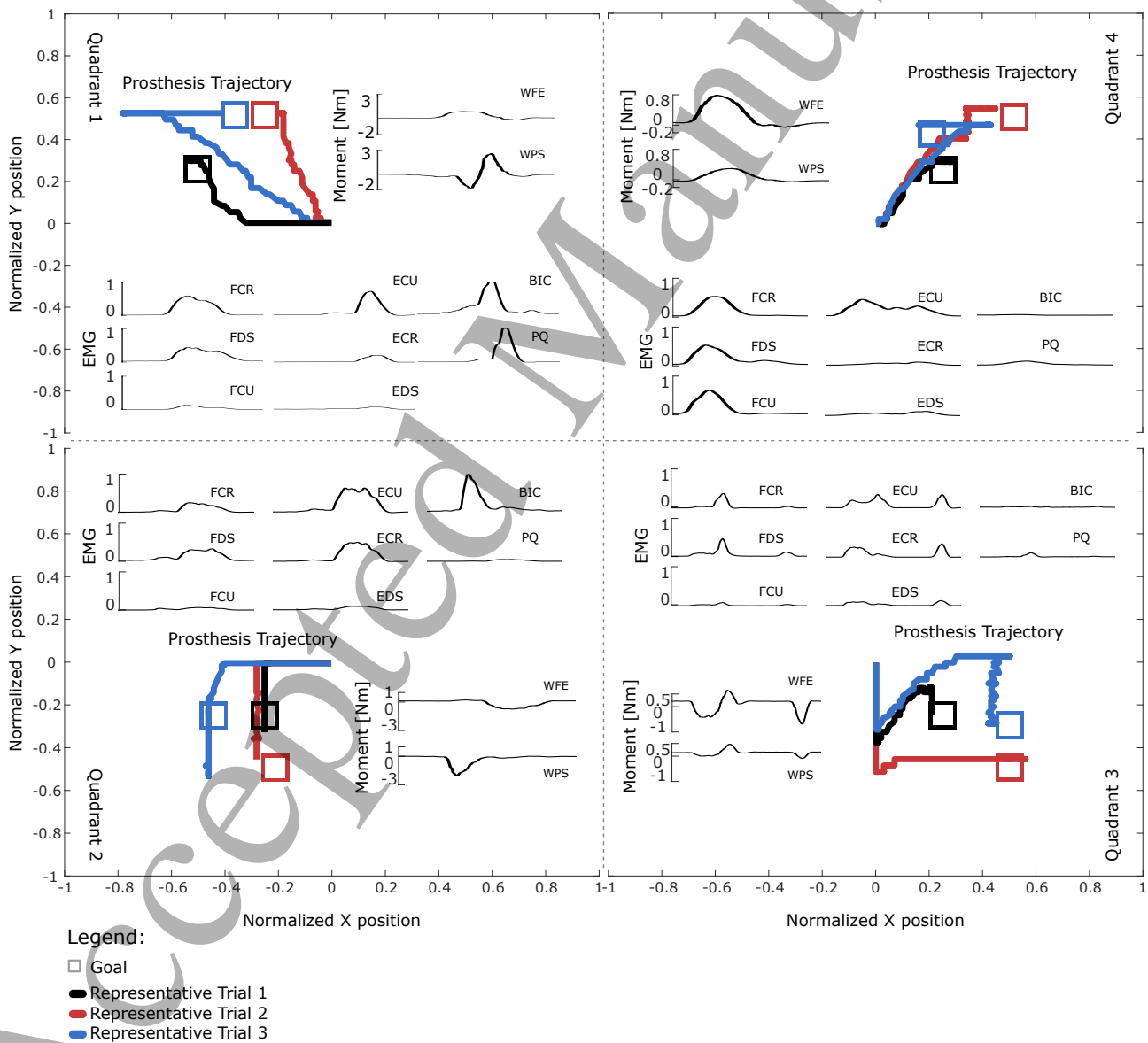


Figure 4. Diagonal target reaching tests reported for the transradial amputee (TR1). Results are reported for each of the four quadrants. See Movie 1 for a visual example of quadrant 3 reaching tasks. Three representative targets per quadrant are depicted as square-shaped cursors. Each target is reached from the same initial position, i.e. zero degrees of wrist flexion and forearm pronation (hand neutral position). The target workspace spanned the interval $[-1, 1]$ in normalized units in vertical and horizontal directions, where -1 and 1 corresponded to full pronation/flexion and supination/extension of the prosthesis. Each target is reached by the simultaneous control of two degrees of freedoms (DOFs). In each quadrant, each target is represented along with the underlying electromyograms (EMGs) recorded from the residual forearm muscles including: flexor/extensor carpi radialis (FCR/ECR), flexor/extensor carpi ulnaris (FCU/ECU), flexor/extensor digitorum superficialis (FDS/EDS), pronator teres (PT), and biceps brachii (BIC). Furthermore, the resulting DOF moments predicted at the phantom limb wrist flexion-extension (WFE) and forearm pronation-supination (WPS) DOFs are depicted, i.e. see black curves in each quadrant. Across all quadrants and targets, vertical and horizontal directions are achieved by controlling WFE and WPS respectively. EMGs are depicted as dimensionless curves whereas moments (torques) are represented in Nm.

Virtual Target Reaching Tasks

During the **virtual target reaching tasks**, subjects sat in front of a monitor and were asked to position themselves on the chair so that their right arm could move freely in any direction. The monitor provided visual feedback in the form of a ball-shaped cursor representing the prosthesis wrist flexion-extension and pronation-supination kinematics state. Subjects were instructed to move a ball-shaped cursor to reach a square-shaped target while keeping the cursor within the target for more than 1 second. Both cursor and target moved in a Cartesian space. Cursor vertical movements were accomplished by actuating the prosthesis wrist flexion-extension DOF via appropriate muscle contractions. Flexion and extension moved the cursor in the negative and positive vertical directions respectively. Similarly, cursor horizontal movements were accomplished by actuating the prosthesis wrist pronation-supination DOF. Pronation and supinations moved the cursor in the negative and positive horizontal directions respectively. Prosthesis neutral position corresponded to the cursor being in the Cartesian space origin. During all tasks, the myoelectric prosthesis was located next to the subject.

The workspace spanned the interval $[-1, 1]$ in normalized units in vertical and horizontal directions, where -1 and 1 corresponded to full pronation/flexion and supination/extension of the prosthesis. The prosthesis wrist range of motion was $[-150, 150]$ and $[-75, 50]$ degrees for pronation/supination and flexion/extension respectively. Tasks were conducted with variable travel distance that ranged between 0.35 and 0.7 normalized units and with constant target size of 0.2 by 0.2 normalized units. The targets were centered at the coordinates $(\pm 0.25, \pm 0.25)$, $(\pm 0.25, \pm 0.5)$, $(\pm 0.5, \pm 0.25)$, and $(\pm 0.5, \pm 0.5)$, where the signs of the coordinates were determined by the quadrant that was tested. Subject performed two series of tests.

The first test series verified the system robustness to hand movement artefacts. Subjects were required to repeatedly open and close their right biological or phantom hands in time to an acoustic metronomic cue, i.e. 50 beats per seconds, 10 repeated hand opening and closings. The subjects were instructed to exert 10% of their maximum opening\closing force.

The second test series verified the system ability to enable controlling WFE and WPS individually, sequentially, as well as simultaneously. Subjects were required to perform a number of reaching tests. Each test required reaching eight targets randomly located on the:

- Vertical axis only, i.e. prosthesis WFE DOF myoelectric control.
- Horizontal axis only, i.e. prosthesis WPS DOF myoelectric control.
- Cartesian space four quadrants using sequential control of prosthesis WFE and WPS DOFs.
- Cartesian space four quadrants respectively, i.e. top-left, bottom-left, top-right, bottom-right. Each quadrant required the simultaneous and proportional control of the prosthesis WFE and WPS DOFs.

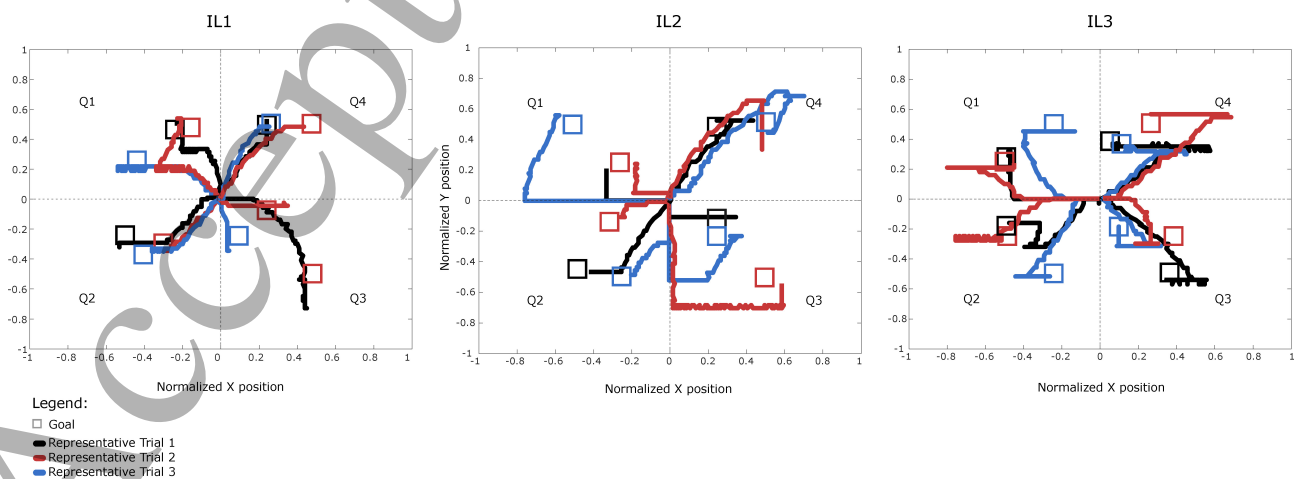
Importantly, in all the tests, the subjects could activate the DOFs simultaneously, but during horizontal, vertical and sequential task, they were instructed to use a single DOF at a time. The aim of these tests was to assess the selectivity of control and the amount of cross talk between the command signals (unwanted activation). Each test series was repeated with the right arm in three different postures including: fully extended elbow, 90 degree flexed elbow, 90 degree flexed elbow and 90 degree abducted shoulder. Arm postures were monitored via inertial measurement units (XSens, Enschede, Netherlands) placed in the correspondence of anatomical landmarks including: right acromion, humerus lateral compartment, forearm lateral compartment. Moreover, each test was performed both using our proposed model-based system as

well as the classic commercial control system. The aim was to compare the performance of the novel method to that of the commercial benchmark.

Clothespin Task

During the clothespin task subjects wore the prosthesis, which was connected to their forearms. For the able-bodied subjects, the prosthesis was connected to a custom-made splint, which was then strapped to the forearm. For the amputee subject, the prosthesis was mounted to a custom-made socket (as in a real-life application). They stood in front of a clothespin test preparation platform. These tasks verified the ability to accurately control WPS and HOC simultaneously and proportionally during functionally relevant tasks. Each test was performed both using our proposed model-based system as well as the classic commercial control system. Subjects performed two series of tests. The first test series involved grasping 12 pins located on horizontal bars and placing them onto a vertical bar. Each pin triplet underlay different stiffness, hence the need for grips with different force levels. This test was designed so that the subject needed to activate WPS as well as HOC proportionally (to modulate force) and simultaneously (to activate multiple DOFs).

The second test series was a variation of the first. It involved performing a clothespin task with pins equipped with custom-made contact sensor and an LED. When the pin fully closed, the sensor activated the LED indicating that the exerted grasping force was too high, thereby “breaking” the “object”. The goal is to grasp five pins each of which of different stiffness while accurately fine-tuning the grip force in order to always keep it below a predefined threshold. More specifically, the subjects needed to exert enough force to open the pin and remove it from the bar, but at the same time, the force had to be below the “breaking” threshold of the pin. Therefore, each pin corresponded to a target window of grasping force.



1
2 371 **Figure 5. Diagonal target reaching tests reported for three intact-limbed individuals (IL1-3).** Three
3
4 372 representative targets per quadrant (Q1-Q4) are depicted as square-shaped cursors. Each target is reached
5
6 373 from the same initial position, i.e. zero degrees of wrist flexion and forearm pronation (hand neutral
7
8 374 position). The target workspace spanned the interval $[-1, 1]$ in normalized units in vertical and horizontal
9
10 375 directions, where -1 and 1 corresponded to full pronation/flexion and supination/extension of the prosthesis.
11
12 376 Each target is reached by the simultaneous control of two degrees of freedoms (DOFs). Across all quadrants
13
14 377 and targets, vertical and horizontal directions are achieved by controlling WFE and WPS respectively. Also
15
16 378 see Movie 1 for a visual example of Q3 reaching tasks.
17
18
19 379

20
21 380 **Functional Tasks**
22

23 381 During the **functional tasks**, each subject wore the prosthesis and stood in front of a shelf. These tasks
24
25 382 verified the system ability of performing real-world functions robustly and intuitively. The tasks were
26
27 383 performed solely by using our proposed model-based system. Subjects performed three testing series. The
28
29 384 first was a block-turn task [43] involving a sequence of fine control actions including: grasping a narrow
30
31 385 wooden block placed on a high self, rotating it of 90 degrees, placing it back on the shelf, re-grasping the
32
33 386 block, rotating it back of 90 degrees, and replacing the block back to its initial position.
34
35

36 387 The second involved grasping a variety of objects ranging from small size and weight to large size and
37
38 388 weight: including an egg and a big bottle (1.5L). This investigated the system robustness in handling heavy
39
40 389 objects or preserving precise grip forces while handling delicate objects (i.e. eggs).
41

42 390 The third assessed the robustness of the system to EMG movement artefacts. It involved mechanical
43
44 391 perturbation in the EMG wired system to induce cable movement. This assessed whether the prosthesis
45
46 392 would be inadvertently activated (by movement-induced noise) and whether the user could still actively
47
48 393 control the prosthesis during the high noise condition.
49
50
51
52
53
54
55
56
57
58
59
60

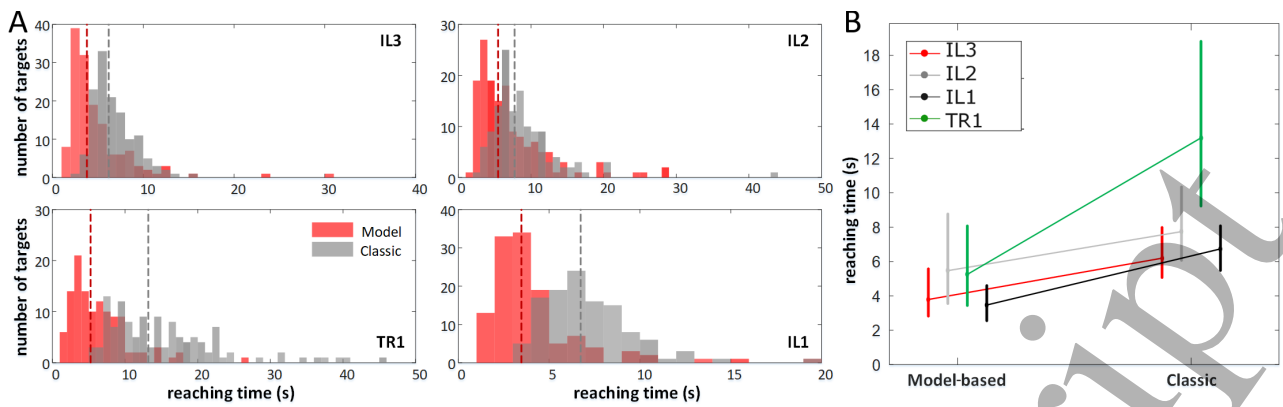


Figure 6. Speed performance during diagonal target reaching test reported for the transradial amputee (TR1) and for the three intact-limbed individuals (IL1-3). (A) Histograms report the distribution of reaching time across all targets for each subject individually, i.e. TR1 and IL1-3. Vertical dotted lines represent median reaching time. (B) Graphs report median (ball marker) and interquartile range (vertical line) of the time took to reach all targets as reported on a subject-specific basis. Targets in each quadrant and condition were accomplished both using our proposed model-based approach (model) as well as the classic commercially available system (classic).

Numerical Analysis

We quantified our proposed model-based framework real-time computation performance using metrics including: the mean computation time, standard deviation, median and 1st-3rd interquartile range measured across all simulation frames from all subjects and tasks. The 90% confidence interval was estimated for our proposed framework computation time using the Chebyshev's theorem, i.e., expected interval = mean \pm 3.16·std. This could be applied with no assumption on the normality of computation time distributions. Path similarity between reaching trajectory and shortest path was calculated using the coefficient of determination (R^2 , square of the Pearson product moment correlation coefficient). In all the reaching tasks, we have determined the mean and standard deviation for the time to reach the target. The outcome measure in the clothespin task was the number of pins transferred per minute.

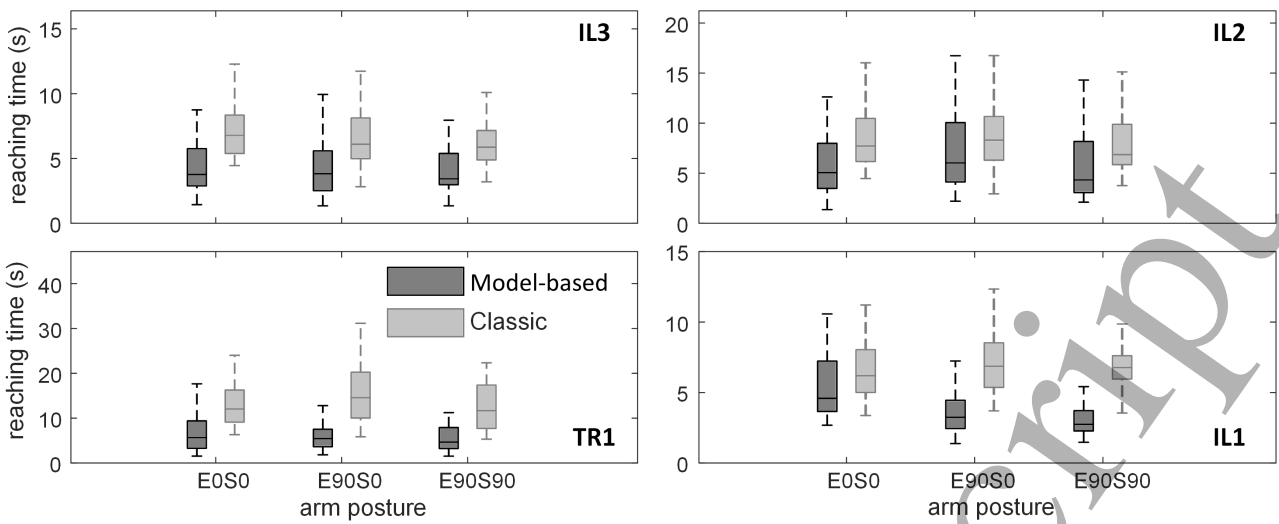


Figure 7. Speed performance as a function of arm position reported for the transradial amputee (TR1) and for the three intact-limbed individuals (IL1-3). Graphs report median (horizontal line), interquartile range (box), and overall max/min values (vertical dotted lines) of the time took to reach diagonal targets as a function of arm configurations: elbow/shoulder 0 degrees (E0S0)), elbow 90 degrees flexed, shoulder 0 degrees (E90S0), elbow 90 degrees flexed, shoulder 90 deg abducted with hand closed (E90S90). Targets in each quadrant and condition were accomplished both using our proposed model-based approach (model-based) as well as the classic commercially available system (classic).

RESULTS

Our proposed real-time musculoskeletal model successfully converted EMG signals from eight forearm muscle groups into mechanical forces produced by 12 musculotendon units or MTUs (Table I) and into resulting EMG-dependent joint moments across a large repertoire of wrist-hand movement (Fig. 1A). EMG-driven model-based joint moment estimates were translated into prosthesis control commands (Fig. 1B), which resulted in the prosthesis moving naturally with no need for explicit angular position control. The prosthesis movement emerging from these commands was directly used to update the kinematic-dependent state in the musculoskeletal model (Fig 1C).

Results showed that our proposed paradigm enabled accurate and robust control of prosthesis WFE and WPS across a large repertoire of tasks performed at different arm configurations (Figs 3-7, Movie 1). Moreover, results showed the ability of natural control of WPS and HOC during functionally relevant clothespin tests (Figs 8, Movies 2-3) and object manipulation tests (Movies 4-7). These tests underwent

dynamic stump-prosthesis movements, enabling testing robustness to EMG non-stationarities (due relative movement between muscle fiber and electrodes) and control precision in the force domain. For all subjects, model calibration (Fig. 2) was always performed a number of days prior to real-time prosthesis control experiments. This provided evidence of the framework ability of retaining subject-specific parameter consistency across time scales, i.e. the model needed to be established once for all per subject. Subjects controlled the prosthesis throughout three series of tasks including: virtual target reaching, clothespin, and functional tasks. This Section presents quantitative results as well as the framework computational times across all series of tasks. In the reminder of this section the three intact-limbed individuals will be referred to as IL1, IL2, and IL3 respectively. The transradial amputee will be referred to as TR1 as indicated in Table II.

Virtual Target Reaching Tasks

The virtual target reaching tasks tested whether the proposed framework enabled subjects to control prosthesis WFE and WPS individually, sequentially, as well as simultaneously. Subjects sat in front of a monitor and were instructed to move a virtual ball-shaped cursor to reach a square-shaped target and keep the cursor within the target for ~1 second. Cursor movements were accomplished by actuating prosthesis WFE and WPS DOFs via forearm muscle contractions. Since it is known that arm posture greatly affects the performance of state of the art decoders [2], we quantified our system robustness to arm configuration, i.e. each test was repeated with the right arm in three postures: (a) fully extended elbow, (b) 90-degree flexed elbow, and (c) 90-degree flexed elbow and 90-degree abducted shoulder.

During the virtual target reaching tasks subjects reached a total of 672 targets, i.e. 168 targets per subjects on average. The first three series of tests verified the precision in controlling WFE and WPS individually (i.e. first and second series, see Methods Section) as well as sequentially (i.e. third series, see Methods Section) in order to reach vertically and/or horizontally displayed targets. Importantly, in all three series, the system always allowed simultaneous DOF control, but subjects were instructed to activate the DOFs individually, testing thereby the ability for selective control. Fig. 3 depicts vertical and horizontal reaching trajectories (i.e. individual DOF control) reported for TR1 along with recorded EMGs and estimated WFE and WPS moments driving the prosthesis movement. Subjects always reached targets using linear trajectories thereby successfully actuating a single DOF at a time with high precision. Path similarity was always accomplished with $R^2 > 0.98$ across all targets and subjects. Intact-limbed individuals and transradial

amputee reached all targets with comparable times (median\interquartile range) during the individual and sequential DOF (two DOFs controlled in sequence) control tasks: 2.2\1.6s (individual) and 4.6\3.1s (sequential) across IL1-3 whereas 2.3\1.6s (individual) and 7.1\5.1s (sequential) for TR1.

The fourth series of tests verified the system ability to enable controlling WFE and WPS simultaneously. Movie 1 shows the proposed model-based framework operated in real-time for the control of the prosthesis by IL1, displaying both musculoskeletal model, recorded EMGs and estimated wrist moments. The movie also shows the concurrent control of the ball-shaped cursor for reaching a variety of diagonal targets (see user interface on external screen). Note that the cursor diagonal trajectories directly correspond to the prosthesis simultaneous actuation of WPS and WFE. Fig. 4 further depicts diagonal reaching trajectories reported for TR1 along with recorded EMGs and estimated WFE and WPS moments driving the prosthesis movement. Fig. 4 shows highly coupled production of WFE and WPS moments underlying simultaneous control of prosthesis DOFs. Moment generating patterns were substantially different during the sequential DOF tasks (Fig. 3), i.e. reduced degree of WFE and WPS moment coupling. Fig. 5 depicts representative diagonal reaching trajectories for all intact-limbed individuals. Figs 4 and 5 also show that all subjects were able to produce diagonal trajectories. Moreover, each individual displayed ability of generating optimal diagonal trajectories in specific quadrants. TR1 was particularly capable of generating diagonal trajectories in quadrants 1, 3 and 4. IL1 and IL3 were capable of generating diagonal trajectories across all quadrants whereas IL2 in quadrants 2 and 4.

Intact-limbed individuals and transradial amputee reached all targets with comparable times (median\interquartile range), i.e. 3.8\2.8s across IL1-3 and 5.3\4.7s for TR1. Each individual reached targets with substantially less time using our proposed model-based framework (model-based) than when using the classic commercially available two-channel sequential control scheme based on co-contraction (classic). Figs 6A and 6B respectively reports the distribution and median\interquartile range of reaching times across all targets on a subject-specific basis. Across all subjects, quadrant 1 targets were reached (median\interquartile range) in 3.4\2.9s (model-based) and 6.2\3.4s (classic). Quadrant 2 targets were reached in 4.1\3.4s (model-based) and 5.9\2.6s (classic). Quadrant 3 targets were reached in 3.4\2.2s (model-based) and 7.4\3.7s (classic). Quadrant 4 targets were reached in 4.2\3.9s (model-based) and 5.8\2.4s (classic).

Importantly, the performance of the proposed model-based approach was preserved across all arm postures. Fig. 7 reports reaching times across arm postures and specifically for each subject. This shows our

proposed model-based approach has no performance decay across arm configuration and consistently outperforms the robust classic control scheme. In this, reaching times were always smaller using the model-based approach than when using the classic control scheme. Across all subjects, reaching times during extended elbow posture were (median\interquartile range) 3.1\2.2s (model-based) and 7.1\3.8s (classic). During elbow flexed arm posture they were 3.4\3s (model-based) and 6.2\4.9s (classic). Finally, during elbow flexed and shoulder abducted arm posture they were 3.3\2s (model-based) and 5.9\3.7s (classic).

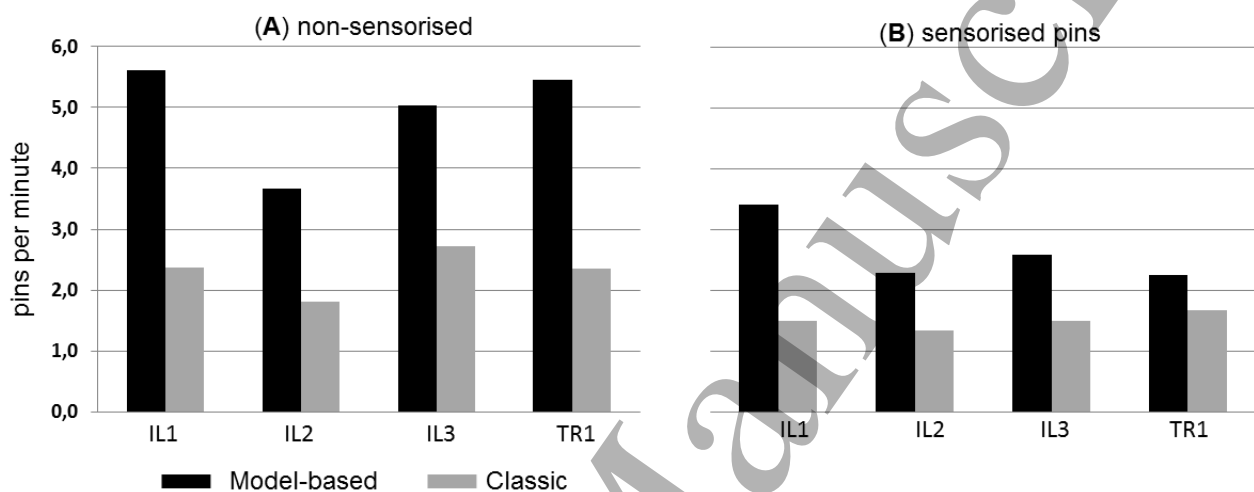


Figure 8. Speed performance during clothespin test. Performance is evaluated in terms of number of clothespins correctly picked and placed per minute (ppm) both using our proposed system (model-based) and the commercially available system (classic). Results are reported for three intact-limbed individuals (IL1-3) and one transradial amputee (TR1). Also refer to Table II. (A) Results are reported for the non-sensorised pin test. (B) Performance is evaluated in terms of number of sensorised clothespins correctly picked without triggering light sensor.

Clothespin Task

The clothespin task verified the ability to accurately control WPS and HOC simultaneously and proportionally across functionally relevant tasks. Subjects performed two series of tests with different pin types. Subjects picked a total of 48 non-sensorised pins (i.e. 12 pins per subject) and a total of 20 sensorized pins (i.e. 5 pins per subject).

The first series of tests (Movie 2, Fig. 8A) involved picking and placing non-sensorised pins (see Methods Section). Pins were arranged in four triplets of different stiffness as previously reported [44].

Results showed that both intact-limbed and amputee individuals could control prosthesis WPS and HOC simultaneously while generating natural motions. This enabled individuals to complete the test with an average speed of 5.24 ± 0.9 pins per minute (ppm) using the proposed model-based framework. In this, the amputee's speed performance (5.5 ± 0.4 ppm) was comparable to that of subject IL1 (5.6 ± 0.7 ppm) and higher than that of subjects IL2 (3.67 ± 0.5 ppm) and IL3 (5.03 ± 0.6 ppm). Each individual completed the test with substantially better performance than when they used the commercially available sequential control scheme based on co-contraction (Fig. 8A) [9]. For the classic-control scheme, average speed performance was 2.3 ± 0.4 ppm and ranged between 1.8 ± 0.1 ppm (subject IL2) and 2.7 ± 0.2 ppm (subject IL3).

The second series (Movie 3, Fig. 8B) involved picking and placing sensorised pins equipped with custom-made contact sensors. The sensor registered when the pin was grasped with force levels beyond predefined thresholds. This was indicated by activating a LED signaling that the subject would have "broken" the grasped object in the real world. Similarly to the first series, test underlay five pins of different stiffness as previously reported (see Material and Methods Section) [44]. The aim was to pick each pin while accurately controlling grasping force in order to open the pin enough to remove it from the bar but without using excessive forces, which would trigger the light sensor. The target force windows to successfully relocate each pin were 7-15% (yellow pins in Movies 2-3), 13-23% (red pins in Movies 2-3), 23-32% (green pins in Movies 2-3), and 35-43% (black pins in Movies 2-3) of the prosthesis maximum force. Results revealed each individual's ability of fine controlling the prosthesis grip force while simultaneously controlling hand rotation. Movie 3 shows the amputee's ability of grasping sensorized pins with the appropriate force level while preserving the required force level accurately during prosthesis wrist pronation-supination, hence with no unwanted activations, i.e. no cross talk across DOFs. Individuals completed the sensorized clothespin test with an average speed of 2.7 ± 0.4 pins per minute (ppm) using the proposed model-based framework (Fig. 9). In this, the amputee's speed performance (2.25 ± 0.1 ppm) was comparable to that of intact-limbed subject IL2 (2.28 ± 0.2 ppm) IL3 (2.58 ± 0.2 ppm) while IL1 (3.4 ± 0.2 ppm) displayed the best performance. Similarly to the first test, each individual completed the test with better performance than when they used the commercially available sequential control scheme based on co-contraction (Fig. 9) [9]. For the classic-control scheme, average speed performance was 1.5 ± 0.13 ppm and ranged between 1.3 ppm (subject IL2) and 1.6 ppm (subject TR1).

Functional Tasks

The functional tasks verified the system ability of performing real-world functions robustly and intuitively and were performed only with the proposed model-based control scheme. Results are reported in the form of a large repertoire of videos. In this, the transradial amputee could successfully perform tasks involving fine control actions (Movies 4-5) as well as manipulation of different objects (Movies 6-7). Fine control actions are displayed in Movie 4, showing TR1 executing a block-turn task involving fine control of HOC and WPS DOFs in the precise positioning of a narrow wooden block in equilibrium on a wooden shelf. Movie 5 shows TR1 precisely controlling HOC DOF force for grasping an egg. The movie shows TR1 ability of grasping force fine control while rotating the prosthetic wrist without breaking the egg. It is worth stressing that this task was performed with no force feedback provided to the amputee. Movie 7 shows how our proposed system was transparent to mechanically induced EMG movement artefacts, preventing inadvertently activating the prosthesis DOFs, i.e. by the resulting noise. Remarkably, the proposed system always enabled amputee's voluntary prosthesis control under high movement-artefact contaminated condition. Finally, the system proved to be robust to highly dynamic movements including grasping and manipulating heavy objects (i.e. a 1.5L water bottle, Movie 7), a tasks that would be challenging for state of the art non-invasive myoelectric systems due to underlying alterations in EMG patterns in response to object weight [2,9,11].

Computational Time

Across all subjects and tests the proposed framework generated prosthesis control commands with average speeds 35 ± 11 ms. This includes the total net delay from the EMG recording to final prosthesis actuation. In this, 90% of control commands produced in one single time frame were generated within 55 ms. This is well within the human perceivable delay in motor execution [45,46].

DISCUSSION

We presented a paradigm of man-machine interfacing where the complete information extracted from an individual's composite neuromusculoskeletal system (i.e. from neuromuscular activation to skeletal joint mechanics) is used to control a robotic multi-functional prosthetic limb. We tested this paradigm on three intact-limbed individuals and on one transradial amputee during a range of tasks involving real-time control

of a physical prosthesis. The results showed performance and control capabilities superior than state of the art non-invasive myocontrol approaches.

Our proposed neuro-mechanical interface addressed a major limit in current state of the art decoders, i.e. the inability of synthesizing the mechanisms that the neuro-musculo-skeletal system uses to control biological joints. State of the art consolidated approaches to the control of artificial limbs are based on machine learning for establishing a single mapping function between EMG and joint kinematics. In this context, there currently exist commercial systems based on pattern recognition (e.g. Coapt LLC) that showed important clinical use [47,48]. Moreover, recent regression based methods have shown levels of robustness to noise [49]. However, current machine learning approaches still display sensitivity to electrode replacement as well as lack of robustness to arm postures, thus providing control paradigms that are sensitive to external conditions.

We propose an alternative idea based on a biomimetic model-based decoder, i.e. a computational model that explicitly synthesizes the dynamics of the musculo-skeletal system as controlled by neural surrogates, i.e. EMG-derived muscle activation signals (Fig. 1). Although online modelling was previously employed in lower limb prostheses [50] and robotic exoskeleton [51,52] scenarios, our study proposes a paradigm never presented for online myoelectric prosthesis control in transradial amputees. Forearm EMG recordings are used to drive forward physiologically correct models of the human musculoskeletal system in real-time, rather than regressing “all the way to” joint angles. This provides a completely new approach to decode amputees’ phantom limb function and concurrently control upper limb prostheses. This model-based biomimetic approach enabled for the first time decoding a transradial amputee’s phantom limb mechanical moments (Figs 3-4) and concurrently mimicking biological wrist function in artificial limbs in real-time (Movies 1-7). Whether joint moments could be reliably decoded from an amputee’s residual muscles EMG to robustly control a prosthetic wrist-hand represented an unanswered scientific question that this work directly addressed. In our paradigm, the prosthesis is the physical device that converted EMG-predicted joint moments into joint angles, thus eliminating the need for numerically integrating dynamic equations of motions. This is different from current solutions operating at the kinematic-level, including (1) model-free decoders, sensitive to unseen motor tasks and time scales [5] and model-based methods [21] that integrate forward dynamic equations of motion, which is a computationally expansive and numerically unstable step [23].

Removing the need for integrating the equation of motion is central for simulating large-scale models, an important element especially relevant for individuals who underwent targeted muscle reinnervation surgical procedures, who require regaining control of large sets of skeletal DOFs. Our proposed biomimetic model-based approach enables control intuitiveness. In this, subjects do not have to learn to produce a specific EMG pattern for prosthesis control. They only need to move their own biological or phantom limb, whose mechanical function is directly captured by the neuro-mechanical interface and concurrently rendered in the real-world by the controlled prosthetic limb.

Results have demonstrated that our method provided an advanced and reliable prosthesis control across tests involving reaching ~600 virtual targets from three arm postures, manipulation of 48 non-sensorised clothespins, 20 sensorised clothespins as well as manipulation of real-world objects during tasks mimicking daily living scenarios. The subjects could successfully activate prosthesis DOFs simultaneously (WFS and WPS, WPS and HOC) across a large range of tasks, and they could proportionally modulate the ratio of the DOF activations, as demonstrated by the diagonal trajectories with different slopes in Figs 4-5. Furthermore, subjects successfully activated single DOFs and transitioned between DOFs sequentially, with minimal cross talk between DOF-specific command signals, which has shown to be a challenge for regression-based methods [53]. Our method consistently and significantly outperformed commercially available benchmark systems (i.e. robust two channel command interface, commercial benchmark) during multi-DOF tasks but also during single-DOF tasks where commercial benchmarks would be expected to best perform. This was evident in the case of the amputee subject, an especially encouraging result.

Fig. 3 shows that in some cases, subjects did not reach a given target via a single muscle contraction but rather via a sequence of brief contractions. This resulted in a number of trajectories underling a sequence torque pulses, dictating virtual cursor movement along a straight path with a variable velocity. Future work will assess whether practice will enable subjects to minimize the number of contractions needed to reach a give target. Fig. 4, shows that certain DOF combinations were achieved via minimally overlapped moment curves. While this is in line with literature studies on natural wrist rotations [54–58], it may also be a consequence of the fact that certain DOF-combinations are more intuitive than others. This may be especially relevant for the amputee subject who performed the tasks with no visual feedback on the prosthesis (please see Movie 1). Future work will also assess to what extent the lack of intrinsic muscle EMGs may contribute to decoded joint moments across coordinated wrist-hand tasks.

Our proposed approach demonstrated decoding robustness across a large variety of wrist-hand tasks (Movie 1) performed across different arm configurations (Figs. 6-7), and during dynamic tasks (i.e. Movies 4-7). Movie 6 demonstrated our system ability to generate no unwanted prosthesis movement when EMG electrode cables underwent mechanically induced movement artefacts. Although this is not representative of commercially available systems schemes (i.e. involving no external cables that could be perturbed), these results show the potential robustness of our system to external movement artefact that may nevertheless come from interaction with the environment. Moreover, it enabled performing highly dynamic motor tasks including manipulating heavy objects (Movie 7).

Our system robustness (which was comparable to the most robust benchmark system in the market) derived from the fact that any joint moment estimate must always exist within the musculoskeletal model operational space and be therefore physiologically plausible. This cannot be achieved with current machine learning decoders that, when trained in one condition, would produce unrealistic estimates (i.e. outside the physiological space) in novel conditions. Machine learning decoding solutions are not constrained by any physiologically plausible structure. Our proposed approach establishes a subject-specific model of an individual's musculoskeletal system. In this, the musculoskeletal model linear scaling and parameter non-linear calibration (i.e. see Methods Section, Fig. 2) directly determine how EMG signals are processed by the subject's musculoskeletal system, i.e. how they are converted into muscle force and further projected onto skeletal DOFs. This effectively reduces the space of potential solutions as EMGs can be mapped only onto mechanical forces that are contained within the musculoskeletal model operational space. Current methods map EMG signals into control commands with no physiological constraints, thus dealing with large solution spaces that contain large portions of non-physiologically plausible solutions.

Results were obtained on a small number of subjects. Future work will be directed in testing the generalization of the results to a greater population encompassing subjects with different levels of amputations as well as comparison of our methodology with respect to state-of-the-art pattern recognition techniques. Our proposed method demonstrated applicability in amputees who underwent traumatic injuries. Future work will assess whether this method can be translated to individuals affected by congenital limb absence. This will require a systematic research to investigate whether motor task learning can be induced in such individuals undergoing physiotherapy training coupled with the proposed real-time system. Further research is also needed to investigate to what extent Hill-type muscle models may contribute to reduce EMG

noise artefacts in online myoelectric scenarios. In this context, computational muscle models may enable simulating musculotendon viscoelasticity, which may act as a dynamic filter for reducing the impact of noise remaining in the EMG after linear envelope computation. Although our results provided evidence of robustness to arm configurations further work is necessary to assess robustness to other sources of noise. Future work will also perform systematic analyses to quantify to what extent the model scaling and calibration procedures (see Methods Section) can be retained for a subject across time scales, i.e. involving longitudinal testing over a number of consecutive weeks.

CONCLUSION

This study showed the potential of the proposed control method to enable the first real-time multi-DOF myoelectric technology that decodes an amputee's phantom limb musculoskeletal mechanics and could be employed in real-world scenarios to control a total of three DOFs including forearm pronation-supination, wrist flexion-extension and hand opening-closing. Future work will couple our proposed model-based approach with deconvolution-based decoding of motor neuron discharges from high-density electromyograms and enable bionic limb control in higher-dimensional DOF spaces [1,30]. Integrating model-based paradigms as a mechanism to constrain and control prosthetic wrist-hand rotation within physiologically plausible operational spaces has the potential to bring prosthetic technology closer to match biological joint function with implications for both upper and lower limb rehabilitation technologies. It will enable individuals to control artificial limbs by estimating physiological activations in their residual muscles, hence control intuitiveness. It will enable decoding "any" movement (i.e. not only those learned in a specific regime) because it synthesizes the underlying neuromuscular processes, hence control robustness and extrapolation to unseen conditions. It will enable predicting internal somatosensory variables (i.e. muscle/tendon length, tension), which will help restore amputees' somatosensory processes in advanced closed-loop neuro-prostheses.

REFERENCES

- [1] Farina D, Vujaklija I, Sartori M, Kapelner T, Negro F, Jiang N, Bergmeister K, Andalib A, Principe J and Aszmann O C 2017 Man/machine interface based on the discharge timings of spinal motor neurons after targeted muscle reinnervation *Nat. Biomed. Eng.* **1** 0025

- 1
2 687 [2] Farina D and Aszmann O 2014 Bionic Limbs: Clinical Reality and Academic Promises. *Sci. Transl.*
3
4 688 *Med.* **6** 257ps12
- 5
6 689 [3] Micera S, Rossini P M, Rigosa J, Citi L, Carpaneto J, Raspopovic S, Tombini M, Cipriani C,
7
8 690 Assenza G, Carrozza M C, Hoffmann K-P, Yoshida K, Navarro X and Dario P 2011 Decoding of
9
10 691 grasping information from neural signals recorded using peripheral intrafascicular interfaces. *J.*
11
12 692 *Neuroeng. Rehabil.* **8** 53
- 13
14 693 [4] Kuiken T A, Miller L A, Lipschutz R D, Lock B A, Stubblefi K, Marasco P D, Zhou P, Dumanian G
15
16 694 A, Stubblefield K, Marasco P D, Zhou P and Dumanian G A 2007 Targeted reinnervation for
17
18 695 enhanced prosthetic arm function in a woman with a proximal amputation: a case study. *Lancet* **369**
19
20 696 371–80
- 21
22 697 [5] Jiang N, Dosen S, Muller K R and Farina D 2012 Myoelectric Control of Artificial Limbs: Is There a
23
24 698 Need to Change Focus? [In the Spotlight] *IEEE Signal Process. Mag.* **29** 150–2
- 25
26 699 [6] Hahne J M, Bießmann F, Jiang N, Rehbaum H, Member S, Farina D, Member S, Meinecke F C,
27
28 700 Müller K and Parra L C 2014 Linear and Nonlinear Regression Techniques for Simultaneous and
29
30 701 Proportional Myoelectric Control **22** 269–79
- 31
32 702 [7] Farina D, Jiang N, Rehbaum H, Holobar A, Graimann B, Dietl H and Aszmann O C 2014 The
33
34 703 extraction of neural information from the surface EMG for the control of upper-limb prostheses:
35
36 704 Emerging avenues and challenges *IEEE Trans. Neural Syst. Rehabil. Eng.* **22** 797–809
- 37
38 705 [8] Enoka R M 2008 *Neuromechanics of Human Movement* (Human Kinetics Publishers, Inc.)
- 39
40 706 [9] Jiang N, Dosen S, Muller K R and Farina D 2012 Myoelectric Control of Artificial Limbs: Is There a
41
42 707 Need to Change Focus? [In the Spotlight] *IEEE Signal Process. Mag.* **29** 150–2
- 43
44 708 [10] Ifft P J, Shokur S, Li Z, Lebedev M a and Nicolelis M a L 2013 A brain-machine interface enables
45
46 709 bimanual arm movements in monkeys. *Sci. Transl. Med.* **5** 210ra154
- 47
48 710 [11] Sartori M, Llyod D G and Farina D 2016 Neural Data-driven Musculoskeletal Modeling for
49
50 711 Personalized Neurorehabilitation Technologies *IEEE Trans. Biomed. Eng.* **63** 879–93
- 51
52 712 [12] Lloyd D G and Besier T F 2003 An EMG-driven musculoskeletal model to estimate muscle forces
53
54 713 and knee joint moments in vivo *J. Biomech.* **36** 765–76
- 55
56 714 [13] Sartori M, Reggiani M, Farina D and Lloyd D G 2012 EMG-driven forward-dynamic estimation of
57
58 715 muscle force and joint moment about multiple degrees of freedom in the human lower extremity

PLoS One **7** 1–11

- [14] Sartori M, Farina D and Lloyd D G 2014 Hybrid neuromusculoskeletal modeling to best track joint moments using a balance between muscle excitations derived from electromyograms and optimization *J. Biomech.* **47** 3613–21
- [15] Durandau G, Farina D and Sartori M 2018 Robust Real-Time Musculoskeletal Modeling driven by Electromyograms *IEEE Trans. Biomed. Eng.* **65** 556–64
- [16] Manal K, Gravare-Silbernagel K and Buchanan T S 2011 A real-time EMG-driven musculoskeletal model of the ankle *Multibody Syst. Dyn.* **28** 169–80
- [17] Pizzolato C, Reggiani M, Saxby D J, Ceseracciu E, Modenese L and Lloyd D G 2017 Biofeedback for Gait Retraining Based on Real-Time Estimation of Tibiofemoral Joint Contact Forces *IEEE Trans. Neural Syst. Rehabil. Eng.* **25** 1612–21
- [18] Manal K, Gonzalez R V, Lloyd D G and Buchanan T S 2002 A real-time EMG-driven virtual arm. *Comput. Biol. Med.* **32** 25–36
- [19] Chadwick E K, Blana D, van den Bogert A J T and Kirsch R F 2009 A real-time, 3-D musculoskeletal model for dynamic simulation of arm movements. *IEEE Trans. Biomed. Eng.* **56** 941–8
- [20] Crouch D L and He H 2016 Lumped-parameter electromyogram-driven musculoskeletal hand model: A potential platform for real-time prosthesis control *J. Biomech.* **49** 3901–7
- [21] Crouch D L and Huang H (Helen) 2017 Musculoskeletal model-based control interface mimics physiologic hand dynamics during path tracing task *J. Neural Eng.* **14** 036008
- [22] Pan L, Crouch D L and Huang H 2018 Myoelectric Control Based on a Generic Musculoskeletal Model: Toward a Multi-User Neural-Machine Interface *IEEE Trans. Neural Syst. Rehabil. Eng.* **26** 1435–42
- [23] Blana D, Chadwick E K, van den Bogert A J and Murray W M 2017 Real-time simulation of hand motion for prosthesis control *Comput. Methods Biomech. Biomed. Engin.* **20** 540–9
- [24] Durandau G, Farina D and Sartori M Real-time musculoskeletal modeling driven by electromyograms *IEEE Trans. Biomed. Eng.*
- [25] Schaffelhofer S, Sartori M, Scherberger H and Farina D 2015 Musculoskeletal Representation of a Large Repertoire of Hand Grasping Actions in Primates *IEEE Trans. Neural Syst. Rehabil. Eng.* **23**

- 1
2 745 210–20
3
4 746 [26] Sartori M, Reggiani M, Pagello E and Lloyd D G 2012 Modeling the human knee for assistive
5
6 747 technologies. *IEEE Trans. Biomed. Eng.* **59** 2642–9
7
8 748 [27] Sartori M, Reggiani M, van den Bogert A J and Lloyd D G 2012 Estimation of musculotendon
9
10 749 kinematics in large musculoskeletal models using multidimensional B-splines *J. Biomech.* **45** 595–
11
12 750 601
13
14 751 [28] Sartori M, Maculan M, Pizzolato C, Reggiani M and Farina D 2015 Modeling and Simulating the
15
16 752 Neuromuscular Mechanisms regulating Ankle and Knee Joint Stiffness during Human Locomotion *J.*
17
18 753 *Neurophysiol.* **114** 2509–27
19
20
21 754 [29] Sartori M, Llyod D G and Farina D 2016 Neural data-driven musculoskeletal modeling for
22
23 755 personalized neurorehabilitation technologies *IEEE Trans. Biomed. Eng.* **63** 879–93
24
25 756 [30] Sartori M, Yavuz U S and Farina D 2017 In Vivo Neuromechanics: Decoding Causal Motor Neuron
26
27 757 Behavior with Resulting Musculoskeletal Function *Sci. Rep.* **7** 13465
28
29 758 [31] Besier T F, Lloyd D G and Ackland T R 2003 Muscle activation strategies at the knee during
30
31 759 running and cutting maneuvers. *Med. Sci. Sports Exerc.* **35** 119–27
32
33 760 [32] Manal K and Buchanan T S 2003 A one-parameter neural activation to muscle activation model:
34
35 761 estimating isometric joint moments from electromyograms. *J. Biomech.* **36** 1197–202
36
37 762 [33] Shao Q, Bassett D N, Manal K and Buchanan T S 2009 An EMG-driven Model to Estimate Muscle
38
39 763 Forces and Joint Moments in Stroke Patients *Comput. Biol. Med.* **39** 1083–8
40
41
42 764 [34] Higginson J S, Ramsay J W and Buchanan T S 2012 Hybrid models of the neuromusculoskeletal
43
44 765 system improve subject-specificity *Proc. Inst. Mech. Eng. Part H J. Eng. Med.* **226** 113–9
45
46 766 [35] Manal K and Buchanan T S 2005 Use of an EMG-driven biomechanical model to study virtual
47
48 767 injuries. *Med. Sci. Sports Exerc.* **37** 1917–23
49
50 768 [36] Barrett R, Besier T and Lloyd D 2007 Individual muscle contributions to the swing phase of gait: An
51
52 769 EMG-based forward dynamics modelling approach *Simul. Model. Pract. Theory* **15** 1146–55
53
54 770 [37] Hayashibe M and Guiraud D 2013 Voluntary EMG-to-force estimation with a multi-scale
55
56 771 physiological muscle model. *Biomed. Eng. Online* **12** 86
57
58
59 772 [38] Delp S L, Anderson F C, Arnold A S, Loan P, Habib A, John C T, Guendelman E and Thelen D G
60
773 2007 OpenSim: open-source software to create and analyze dynamic simulations of movement. *IEEE*

Trans. Biomed. Eng. **54** 1940–50

- [39] Saul K R, Hu X, Goehler C M, Vidt M E, Daly M, Velisar A and Murray W M 2014 Benchmarking of dynamic simulation predictions in two software platforms using an upper limb musculoskeletal model. *Comput. Methods Biomech. Biomed. Engin.* 1–14
- [40] H.J. Hermens and B Freriks 2017 SENIAM Project *SENIAM Proj.* 1
- [41] Sartori M, Gizzi L, Lloyd D G D G and Farina D 2013 A musculoskeletal model of human locomotion driven by a low dimensional set of impulsive excitation primitives *Front. Comput. Neurosci.* **7** 79
- [42] Sartori M, Maculan M, Pizzolato C, Reggiani M and Farina D 2015 A Theoretical and Computational Framework for Modeling and Simulating Musculoskeletal Stiffness during Locomotion *The 25th Congress of the International Society of Biomechanics* (Glasgow) pp 1–2
- [43] Amsuess S, Vujaklija I, Gobel P, Roche A, Graimann B, Aszmann O and Farina D 2015 Context-Dependent Upper Limb Prosthesis Control for Natural and Robust Use *IEEE Trans. Neural Syst. Rehabil. Eng.* **4320** 1–1
- [44] De Nunzio A M, Dosen S, Lemling S, Markovic M, Schweisfurth M A, Ge N, Graimann B, Falla D and Farina D 2017 Tactile feedback is an effective instrument for the training of grasping with a prosthesis at low- and medium-force levels *Exp. Brain Res.* **235** 2547–59
- [45] Farina D and Sartori M 2016 Surface Electromyography for Man-Machine Interfacing in Rehabilitation Technologies *Surface Electromyography: Physiology, Engineering and Applications* ed D Farina and R Merletti (IEEE/Wiley) pp 540–60
- [46] Parker P, Englehart K and Hudgins B 2006 Myoelectric signal processing for control of powered limb prostheses *J. Electromyogr. Kinesiol.* **16** 541–8
- [47] Kuiken T, Turner K, Soltys N and Dumanian G 2015 First clinical fitting of an individual after bilateral TMR with pattern recognition control *Prosthet. Orthot. Int.* **39** 133
- [48] Hargrove L J, Miller L A, Turner K and Kuiken T A 2017 Myoelectric Pattern Recognition Outperforms Direct Control for Transhumeral Amputees with Targeted Muscle Reinnervation: A Randomized Clinical Trial *Sci. Rep.* **7**
- [49] Hahne J M, Markovic M and Farina D 2017 User adaptation in Myoelectric Man-Machine Interfaces *Sci. Rep.* **7**

1
2 803 [50] Eilenberg M F, Geyer H and Herr H 2010 Control of a powered ankle-foot prosthesis based on a
3
4 804 neuromuscular model. *IEEE Trans. Neural Syst. Rehabil. Eng.* **18** 164–73
5
6 805 [51] Fleischer C and Hommel G 2008 A Human – Exoskeleton Interface Utilizing Electromyography
7
8 806 *IEEE Trans. Robot.* **24** 872–82
9
10 807 [52] Cavallaro E E, Rosen J, Perry J C and Burns S 2006 Real-Time Myoprocessors for a Neural
11
12 808 Controlled Powered Exoskeleton Arm *IEEE Trans. Biomed. Eng.* **53** 2387–96
13
14 809 [53] Farina D, Vujaklija I, Sartori M, Kapelner T, Negro F, Jiang N, Bergmeister K, Andalib A, Principe
15
16 810 J and Aszmann O 2016 Man-Machine Interfacing With Discharge Timings of Spinal Motor Neurons
17
18 811 After Targeted Muscle Reinnervation *Nat. Biomed. Eng.*
19
20
21 812 [54] Formica D, Charles S K, Zollo L, Guglielmelli E, Hogan N and Krebs H I 2012 The passive stiffness
22
23 813 of the wrist and forearm *J. Neurophysiol.* **108** 1158–66
24
25 814 [55] Charles S K and Hogan N 2011 Dynamics of wrist rotations *J. Biomech.* **44** 614–21
26
27 815 [56] Rankin J W and Neptune R R 2012 Musculotendon lengths and moment arms for a three-
28
29 816 dimensional upper-extremity model. *J. Biomech.* **45** 1739–44
30
31 817 [57] Holzbaur K R S, Murray W M and Delp S L 2005 A Model of the Upper Extremity for Simulating
32
33 818 Musculoskeletal Surgery and Analyzing Neuromuscular Control *Ann. Biomed. Eng.* **33** 829–40
34
35 819 [58] Peaden A W and Charles S K 2014 Dynamics of wrist and forearm rotations *J Biomech* **47** 2779–85
36
37
38 820
39

40 821 **COMPETING INTERESTS**

41
42 822 The authors declare no financial competing interests.
43
44 823
45

46 824 **PARTICIPANT CONSENT**

47
48 825 The authors have confirmed that any identifiable participants in this study have given their consent for
49
50 826 publication.
51
52 827
53

54 828 **DATA AND MATERIALS AVAILABILITY**

55
56 829 Data and code are available upon request.
57
58 830
59
60

831 **MOVIES**

Movie 1. Graphical user interface during wrist control tasks. The proposed model-based framework operated in real-time for the simultaneous control of the prosthesis wrist flexion-extension (WFE) and pronation-supination (WPS) by IL1 (Table II). The movie displays the musculoskeletal model, recorded EMGs and estimated joint moments (see laptop) and the concurrent control of the ball-shaped cursor for reaching a variety of diagonal targets (see user interface on external screen). Note that the cursor diagonal trajectories directly correspond to the prosthesis simultaneous actuation of WPS and WFE. After every target is successfully reached, the prosthesis automatically resets to its neutral position.

Movie 2. Non-sensorised clothespin test. The transracial amputee subject picking and placing non-sensorised pins arranged in four triplets of different stiffness as previously reported (22). The amputee controls prosthesis wrist pronation-supination and hand opening-closing simultaneously while generating natural motions.

Movie 3. Sensorised clothespin test. The transracial amputee subject picking and placing sensorised pins of different stiffness. The target force windows to successfully relocate each pin are 7-15% (yellow pin), 13-23% (red pin), 23-32% (green pin), and 35-43% (black pin) of the prosthesis maximum force. The movie shows the amputee's ability of fine controlling the prosthesis grip force while simultaneously controlling hand rotation, while not triggering the light sensor.

Movie 4. Block turn test. The transradial amputee executes a block-turn task involving fine control of prosthesis wrist pronation-supination and hand opening-closing simultaneously in the precise positioning of a narrow wooden block in equilibrium on a wooden shelf.

Movie 5. Egg manipulation. The transradial amputee precisely controls hand opening-closing grip force for grasping an egg. The movie shows the amputee's ability of fine grasping force control while rotating the prosthetic wrist without breaking the egg.

Movie 6. Cable induced movement artefacts. How our proposed system being transparent to mechanically induced cable-related movement artifacts visibly present in the recorded electromyograms. Despite the

1
2 861 artificially induced noise condition the prosthesis does not inadvertently activate unwanted degrees of
3
4 862 freedom. The movie also shows amputee’s voluntary prosthesis control under noise condition.
5
6 863
7
8 864 **Movie 7. Manipulation of heavy objects.** Our proposed system enabling grasping and manipulating heavy
9
10 865 objects including a 1.5L water bottle, a task that would be challenging for state of the art non-invasive
11
12 866 myoelectric systems.
13
14
15
16
17
18
19
20
21
22
23
24
25
26
27
28
29
30
31
32
33
34
35
36
37
38
39
40
41
42
43
44
45
46
47
48
49
50
51
52
53
54
55
56
57
58
59
60